NUCLEAR INSTRUMENTS AND METHODS 68 (1969) 61–69; © NORTH-HOLLAND PUBLISHING CO.

THE ENERGY CALIBRATION OF TANDEM ACCELERATORS*

J. C. OVERLEY†, P D PARKER and D A. BROMLEY

A W. Wright Nuclear Structure Laboratory,

Yale University, New Haven, Connecticut, U.S A

Received 30 September 1968

The beam energy homogeneity, stability and reproducibility of a model MP tandem Van de Graaff accelerator has been investigated. The 90° analyzing magnet system was calibrated using a number of (p,n) thresholds whose proton energies are known absolutely in the range from 4 to 10 MeV. The linearity of the beam momentum analysis system was then checked for higher magnetic rigidities by observing the $^{2}H(^{16}O,n)^{17}F$ neutron threshold for several different ^{16}O ionic charge states. The magnet calibration constant, obtained from a least-squares analysis of the results of threshold measurements for several different reactions, was reapplied to the data to obtain a new set of self-consistent energies for the calibration reactions themselves This procedure, which relies on the assumption that the data are all measures of the same calibration constant, results in smaller statistical errors for the calibration energies than those previously cited. Measurements were then extended using the linearity of the analysis system as established by the $^{2}H(^{16}O,n)^{17}F$ measurements to include the $^{12}C(p,n)^{12}N$, $^{24}Mg(p,n)^{24}Al$, $^{28}Si(p,n)^{28}P$, $^{32}S(p,n)^{32}Cl$ and $^{40}Ca(p,n)^{40}Sc$ neutron thresholds at energies of 19.658 ± 0.005 MeV, 15 286 ± 0.003 MeV, 15.669 ± 0 004 MeV, 13.899 ± 0.014 MeV, and 15 491 ± 0.003 MeV, respectively. With the exception of the $^{32}S(p,n)^{32}Cl$ reaction, for which there are target difficulties, these thresholds provide the first series of calibration points in the energy range from 10 to 20 MeV

1. Introduction

As higher energy accelerators with a high degree of beam energy homogeneity become more available, the need for accurately known beam energy calibration points at high energies will become more acute. Therefore, when the first model MP tandem Van de Graaff accelerator became operational at Yale, a program was instituted to determine accurately the energy calibration of the beam handling system and then, on the basis of this calibration, to investigate additional reactions which had hitherto been inaccessible with precision.

2. Instruments and methods

The model MP tandem Van de Graaff accelerator met its operating specifications about two years ago, producing proton beams with intensities up to 26 μA with the requisite degree of stability and homogeneity. Subsequently, beams of deuterons, ^{3}He, ^{4}He and a variety of heavy ions have been produced and accelerated through terminal potentials ranging from 0.9 to 11.75 MV.

Because of the heavy ion capabilities of the accelerator, the beam optical elements are designed for ion beams with magnetic rigidities equivalent to that for 175 MeV protons. The 90° beam momentum analyzing magnet is double focussing with a nominal radius of curvature $R = 132$ cm. Beam trajectories through the magnet are defined by slits placed at the object and image points, at a distance $2R = 264$ cm from the entrance and exit points of the magnet, respectively. For the experiments described herein these slits were each set with a total separation of 0.76 mm. The field within the magnet is measured with a proton nuclear-magnetic-resonance probe placed near the midpoint of the beam trajectory within the magnet. Detailed field plots, taken before the magnet was installed[+], indicate a field homogeneity of better than ± 1 part in 500 at 12 kG over 90% of the beam orbit, and a differential hysteresis of less than ± 1 part in 10^4 at 5 kG after a 10% field change.

Two methods were used to determine the neutron emission thresholds. For those reactions initiated by oxygen ions or by protons with energies below 6 MeV, neutrons were detected with either a NE-401[§] slow neutron scintillation detector or a standard BF_3 long-counter. For all the other threshold measurements, neutron and gamma-ray backgrounds were found to be prohibitively high, and the delayed counting of decay positrons from shortlived residual nuclei was employed, using a NE-102 plastic scintillator, 7.5 cm long and 5 cm in diameter. The latter technique has the additional advantage that the detection efficiency is constant for a given reaction; the changing of neutron energy and cone angle with incident particle energy is of no concern. All detectors were placed less than 2 cm behind the target so that the solid angle subtended was almost π steradian.

For the delayed counting studies, the proton beam was interrupted by a rotating graphite beam chopper

* Work supported in part by the U. S. Atomic Energy Commission

† Present address: Physics Department, University of Oregon, Eugene, Oregon

+ High Voltage Engineering Corporation, Burlington, Massachusetts, U S.A

§ Nuclear Enterprises Ltd., Winnipeg, Canada.

located immediately beyond the image slits of the analyzing magnet. The chopper was driven at 1800 rpm so that the beam-on and beam-off parts of the cycle were each approximately 8 msec long. During the beam-on portion of the cycle, the beam passed through the target and was stopped in either gold or graphite; scalers and the photomultiplier high voltage were gated off electronically during this portion of the cycle. After the beam was interrupted, the detection systems were reactivated and delayed positrons were counted. The timing signals in the system were derived from a photodiode activated by a light beam which was also intercepted by the mechanical chopper. Backgrounds were reduced by setting a discriminator so that only positrons with energies greater than 5 MeV were recorded. Thus, backgrounds contributed by the $^{13}C(p,n)^{13}N\,(\beta^+\nu)^{13}C$ reaction occurring in the graphite beam stop and the $^{27}Al(p,n)^{27}Si\ (\beta^+\nu)^{27}Al$ reaction, which might have been induced by stray or scattered beam striking the walls of the target chamber, were largely eliminated. The relative efficacy of the different detection methods is illustrated in fig. 1 which shows the $^{58}Ni(p,n)^{58}Cu$ neutron yield and the delayed positron yield from the decay of ^{58}Cu in the vicinity of the threshold.

Standard beam current integration techniques were employed, even for the delayed positron method, and few problems were experienced due to variable beam intensity. The effect of long-lived isotopes producing time-varying backgrounds could be reduced by increasing the positron detection bias.

A liquid nitrogen cold-trap was placed immediately before the target to inhibit build-up of surface layers of carbon. No threshold shifts attributable to this source were observed.

Proton NMR frequencies corresponding to the thresholds were extracted from the yield curves by first subtracting a linearly varying background, determined from the yields below threshold, and then plotting the $\frac{2}{3}$-power of the net yield as a function of NMR frequency (cf. fig. 1). The zero intercept of this curve was taken as the threshold frequency[1]). Although a $\frac{2}{3}$-power linear extrapolation is strictly valid only for $l=0$ neutron emission where the neutron yield is governed solely by phase space factors, the frequency at zero intercept can be determined without ambiguity if the yield above threshold empirically obeys the $\frac{2}{3}$-power law. This is all that is required for calibration purposes as long as the absolute threshold energies are obtained with the same procedures! With this procedure, other small effects such as the "Lewis Effect" [2]), and the influence of beam energy resolution[3]) may also be neglected. Because of these effects, however, conversion of threshold energies obtained in this manner to Q-values or mass excesses can be in error by as much as a few keV.

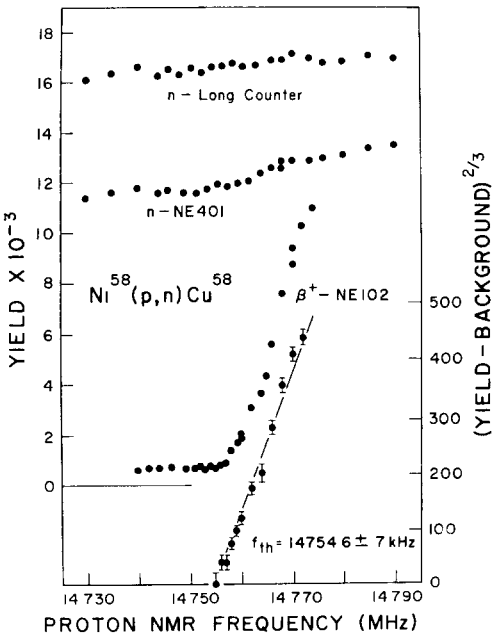

Fig. 1. The $^{58}Ni(p,n)^{58}Cu$ reaction near threshold Neutron yields measured with a BF_3 long-counter and with a NE-401 slow neutron detector are shown together with the delayed positron yield from ^{58}Cu The $\frac{2}{3}$-power of the net positron yield (right-hand scale) is also shown and extrapolated to obtain the threshold frequency.

Fig. 2 shows a thin target neutron yield from the $^{27}Al(p,n)^{27}Si$ reaction. Beam energy stability was checked by setting the beam energy at the midpoint of the sharply increasing yield indicated by the arrow. Neutron yields were determined for a succession of half minute intervals over a two hour period. The variation in the number of neutrons counted per interval is related to the beam energy stability and to statistical fluctuations. The number of times that a given counting rate was obtained is also shown in fig. 2 as a function of counting rate. This indicates, without any modification of operating controls, a beam energy stability very substantially better than 500 eV at 6.0 MeV (or $< 0.01\%$ in frequency) over a two hour period.

Differential hysteresis effects reflecting the analyzing magnet history were found to effect the $^{27}Al(p,n)^{27}Si$ threshold frequency by as much as 0.1%. Fig. 3 illustrates this behavior for a variety of randomly selected prior magnet histories. It was found that reproducibility of $\pm 0.003\%$ could be achieved, however, by an empirically determined recipe which involves bringing the magnet to full field, allowing the field to

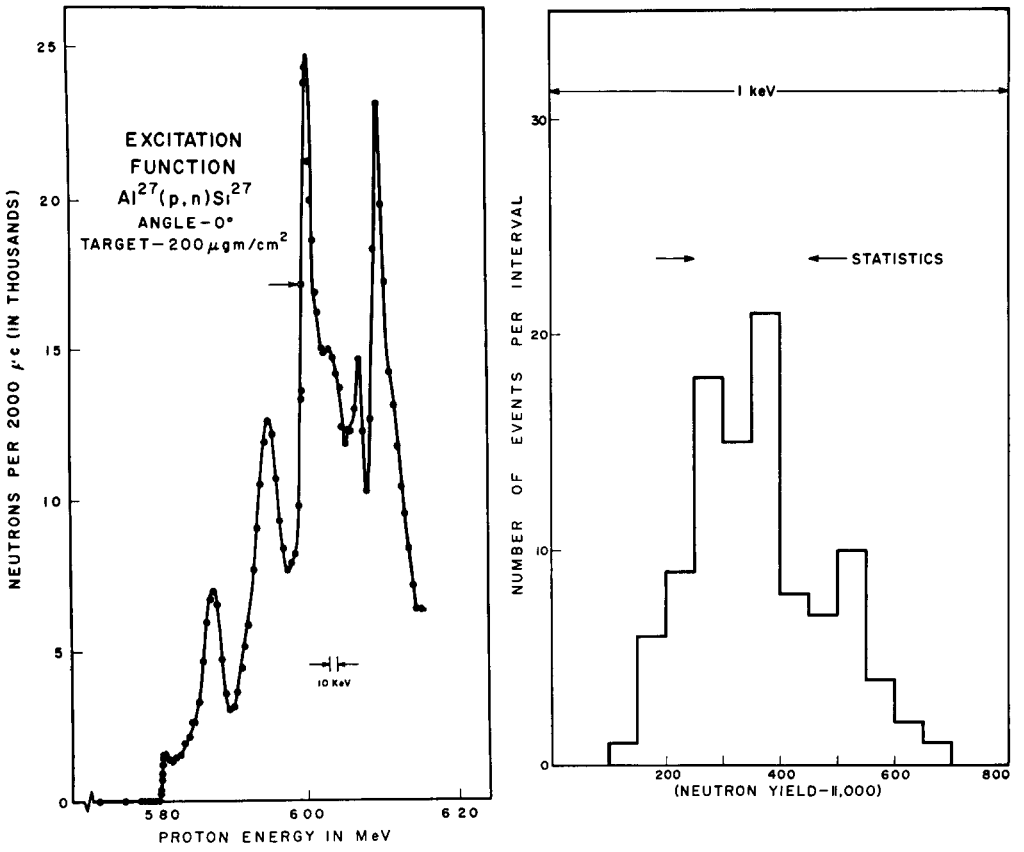

Fig. 2. The thin target neutron yield for the $^{27}Al(p,n)^{27}Si$ reaction. The proton energy was set at the arrow on the side of the sharp resonance peak at 6 MeV. Neutrons were counted for a succession of half minute intervals and the number of times a given neutron yield was measured is plotted against neutron yield at the right Note the suppressed abscissae zero. The spread expected from counting statistics and the shift which would correspond to a 1 keV energy change are indicated.

stabilize there for two minutes, then reducing the field and allowing it to stabilize for two minutes at slightly negative values, and finally increasing the field to the desired value. After this cycling procedure, the field could be changed by $\pm$ 1% without noticeably affecting the measured threshold frequency. No change in this degree of reproducibility was observed over a period of roughly one year.

The threshold frequency for the $^{27}Al(p,n)^{27}Si$ reaction was also investigated for widely differing parameters for injecting the beam into the accelerator and for the high-energy electrostatic beam deflectors which control injection into the analyzing magnet. Shifts in the threshold frequency reflecting these variations were negligible as long as the beam current on target was tuned to a local maximum.

The beam energy resolution, $\Delta E/E$, was estimated at less than 3×10^{-4} on the basis of the deviation from linearity of the $\frac{3}{2}$-power plot of the neutron yield from the $^{7}Li(p,n)^{7}Be$ reaction at threshold. It is of interest to note that the accelerator produced the required beams of protons from 1.88 MeV to 19.66 MeV without requiring any change in configuration or in the pressure of the insulating gas.

3. Results

A summary of the reactions utilized in the energy calibration of the beam handling system is given in table 1. Detection techniques are listed as well as the target materials employed. In the $^{2}H(^{16}O,n)^{17}F$ reaction a deuterated-zirconium target was first employed. However, deuterium inhomogeneities near the front surface of the target necessitated changing to a D_2O ice target. This was formed simply by allowing D_2O vapor to condense in a thin film on a liquid-nitrogen-cooled stainless steel surface. The results obtained with this target are shown in fig. 4.

The threshold frequencies listed in table 1 are the results of several experiments with several different targets employed for each reaction. The uncertainties

listed are derived from the reproducibility of the several experiments and from the estimated uncertainty in extrapolating to zero yield. The latter uncertainty is illustrated in fig. 5 which shows the $^{19}F(p,n)^{19}Ne$ neutron yield and the $\frac{2}{3}$-power of the net yield. The experimental points are shown with statistical counting errors, and two extreme extrapolations to zero net yield are also shown. Since threshold frequency may depend slightly[2,3]) on the extrapolation range, this range is also shown in table 1. In most cases, however,

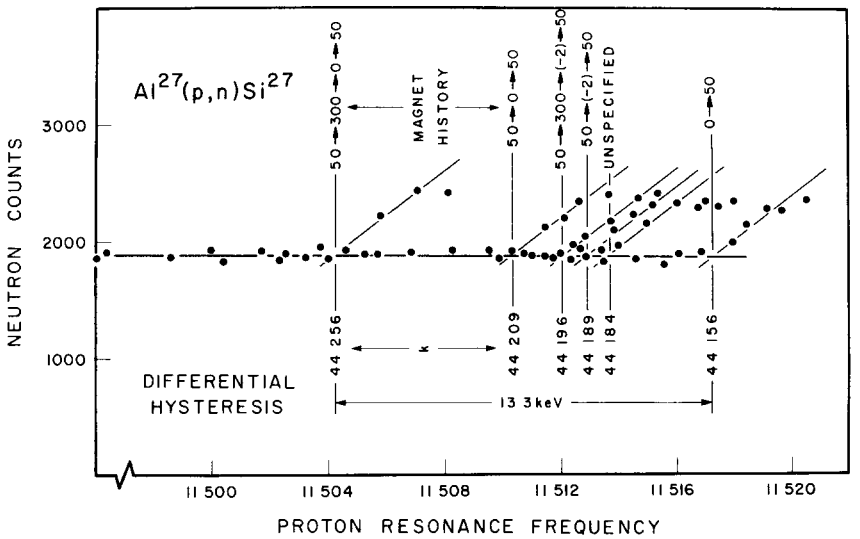

Fig 3. Differential hysteresis measurements on the Yale MP tandem analyzing magnet. Rough determinations of the $^{27}Al(p,n)^{27}Si$ threshold frequency are shown for a variety of indicated prior cycling histories for the analyzing magnet In each case the sequence lists the magnet excitation currents in ampere; 300 ampere corresponds to ≈ 16 kG This figure is intended only to illustrate the magnitude of the differential hysteresis effects and the importance of a specified magnet cycling procedure in obtaining reproducible results. In particular the magnet constant, k, and the actual threshold frequencies are not those arrived at in the final precision determinations

TABLE 1
Calibration reactions

Reaction	Target	Detector	Extrapolation range (keV)	Threshold frequency (kHz)	Energy standard (keV)	Ref.
$^{7}Li(p,n)^{7}Be$	LiF	long-counter	2	6544 2 ± 0.4	1880 60 ± 0.07	1)
$^{13}C(p,n)^{13}N$	graphite	long-counter	5	8589 2 ± 0 7	3235 46 ± 1 1	4), 1)
					3236 9 ± 1.6	3)
$^{19}F(p,n)^{19}Ne$	CaF	long-counter	4	9830 3 ± 0 3	4233.34 ± 1 5	4), 1)
					4234 7 ± 1.0	5)
$^{27}Al(p,n)^{27}Si$	Al foil	long-counter	5	11512.7 ± 0 3	5794.5 ± 2.4	6), 1)
					5802 7 ± 3 4	7), 8)
$^{60}Ni(p,n)^{60}Cu$	99.8% ^{60}Ni	β^+-NE102 n-NE401	10	12675 0 ± 1.0	7023.84 ± 3 9	6), 1)
$^{54}Fe(p,n)^{54}Co$	97.4% ^{54}Fe	β^+-NE102 n-NE401	9	14513.4 ± 0 8	9201.9 ± 3.9	7), 8)
$^{58}Ni(p,n)^{58}Cu$	99.9% ^{58}Ni	β^+-NE102	13	14754 6 ± 0.7	9516 32 ± 3.5	6), 1)
					9512.1 ± 4.1	7), 8)
$^{2}H(^{16}O,n)^{17}F$ (5+)	D_2O-ice	long-counter	120	14502 ± 5	14527 5 ± 5	9)
(4+)			90	18128 ± 3	14528 0 ± 5	
(3+)			100	24171 ± 4	14528.5 ± 5	
(2+)			100	36258 ± 8	14529.0 ± 5	

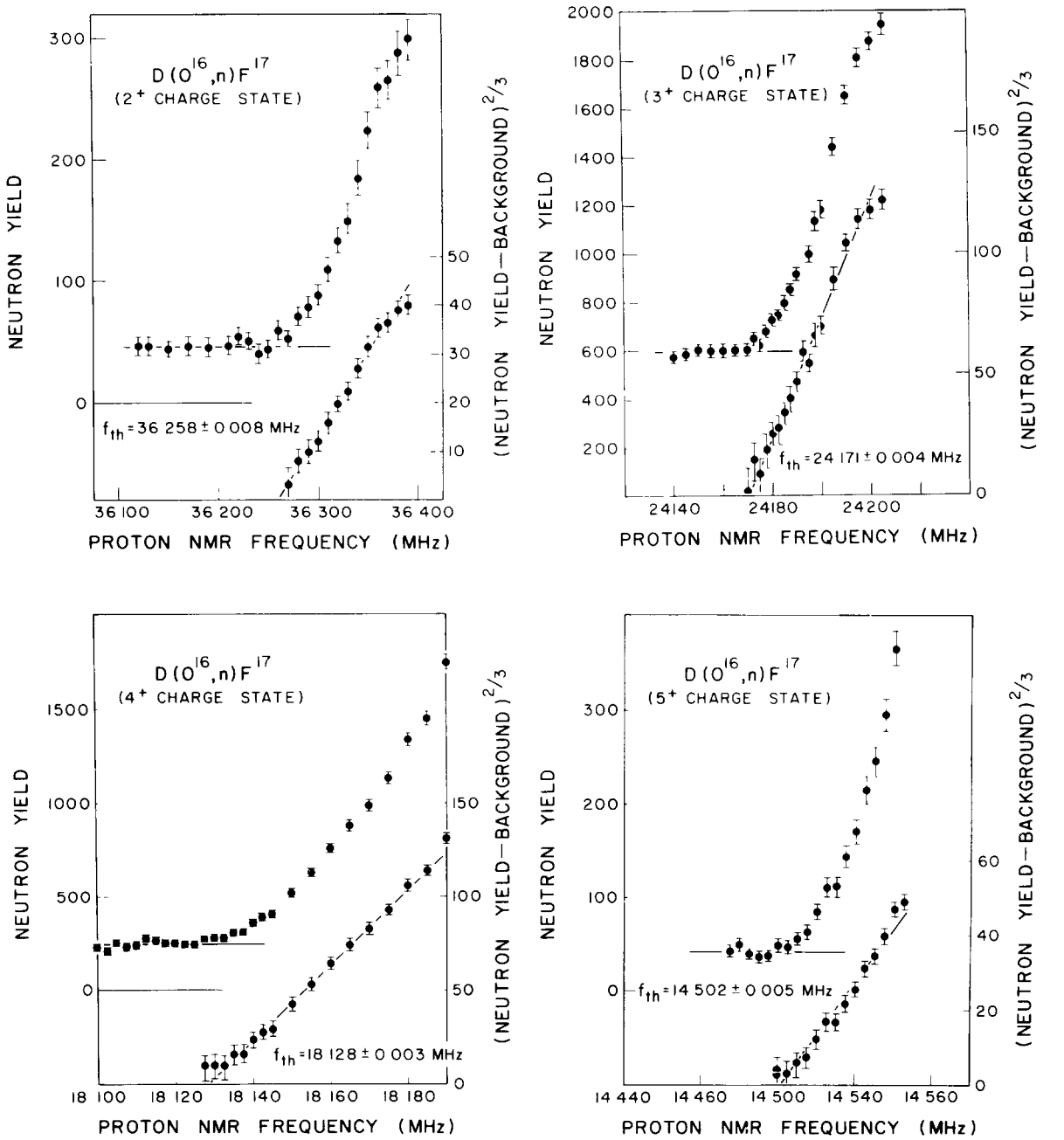

Fig 4 The $^{2}H(^{16}O,n)^{17}F$ neutron yield near threshold for a number of ^{16}O ionic charge states. The $\frac{2}{3}$-power of the net yield is also shown in each case and is extrapolated to yield a threshold frequency. Note that these cases span the equivalent proton energy range from 9 4 to 59 MeV

the extrapolation range is simply the range over which the $\frac{2}{3}$-power of the net yield is linear for the particular targets employed.

The analyzing magnet calibration factor, K, was determined from the threshold frequency, f, from the expression:

$$K = \{ME/(Q^2f^2)\}\{1+E/(2Mc^2)\}, \quad (1)$$

where M, E and Q are the mass (in unified nuclidic mass units), the energy in (keV) and the charge state (in units of the electron charge) of the reaction inducing beam particles while in the analyzing magnet. For the

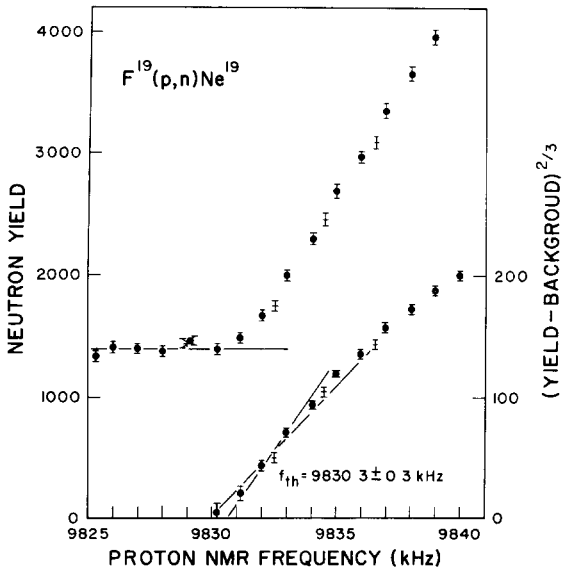

Fig 5. The $^{19}F(p,n)^{19}Ne$ neutron yield near threshold. The $\frac{3}{2}$-power of the net yield is also shown with two extreme linear extrapolations to threshold.

proton induced reactions a mass $M = 1.007277$ u was employed, while for the ^{16}O induced reactions, the appropriate ionic mass was used. This was calculated from an atomic mass[10]) of 15.99491 u by subtracting the mass of the appropriate number of electrons, and neglecting the electron binding energies.

The energy standards, E, used in eq. (1) are also listed in table 1. For the proton induced reactions these are absolute measurements of threshold intercept energies, except for those of Murray et al. which are relative to the well-known ThC and ThC' alpha-particle energies. The $^2H(^{16}O,n)^{17}F$ energies were calculated from the absolute measurement[9]) of the $^{16}O(d,n)^{17}F$ threshold of 1829.2 ± 0.6 keV. This conversion was made using nuclear masses in the kinematics and then increasing the energy obtained by the translational kinetic energy of the ionic electrons. (Very nearly the same result is obtained by using ionic masses in the kinematics.)

The calibration factors obtained are displayed in fig. 6. The uncertainties, ΔK_i, were calculated by quadratically combining the standard deviations listed for the energy standards with the estimated uncertainty due to threshold frequency. In most cases, the major fraction of the uncertainty in K reflects the uncertainty in the energy standard.

The calibration factor decreases with equivalent proton energy from 2 to 4 MeV. This is most probably a result of the rapid onset of saturation of the iron at the entrance and exit edges of the pole faces. As the saturation increases, a higher field is required over the remainder of the orbit (and at the NMR probe position) to maintain the same average field over the trajectory. This postulated saturation effect is in the correct direction whereas other effects which have been considered

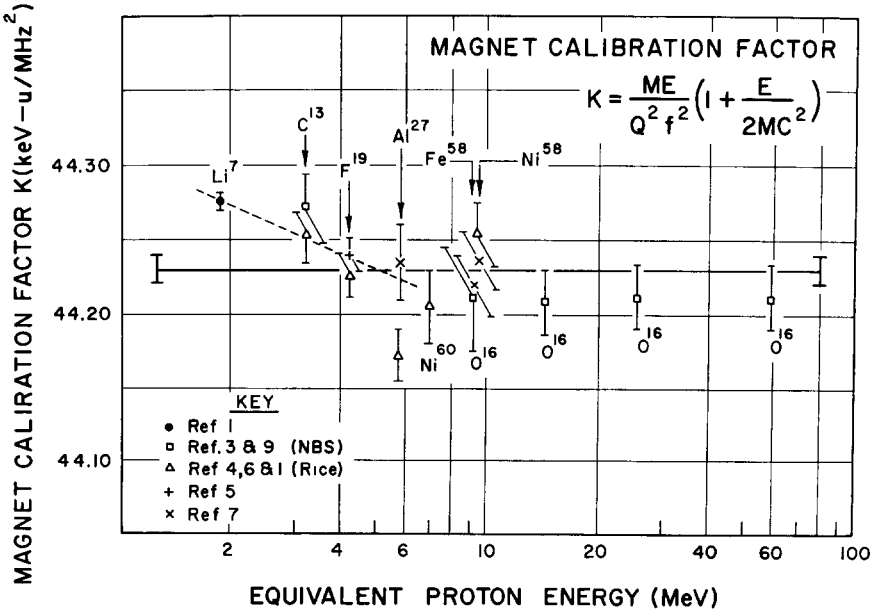

Fig. 6. The magnet calibration factor as a function of equivalent proton energy. The results from absolute measurements of threshold energies by different experimental groups are designated by different symbols. The adopted mean value of the calibration constant and its standard deviation are indicated by the horizontal line and by error bars at the end of the line.

such as target surface contaminations, or residual gas in the vacuum system, would act to depress the calibration factor at low fields. Other similar studies[11-13]) have shown the same effect, and curiously, the effect is of roughly the same magnitude in all cases for quite different magnet configurations.

The threshold measurements made using the $^{2}H(^{16}O,n)^{17}F$ reaction indicate that the calibration factor is constant for proton energies from 9 to 60 MeV, and the other threshold measurements indicate that this factor remains constant down to about 4 MeV. We have made this assumption in calculating an average calibration factor, $\bar{K}$, by the method of least-squares, where $\bar{K}$ is given by

$$\bar{K} = \sum W_i K_i / \sum W_i \text{ and } W_i = (\Delta K_i)^{-2}.$$

All data above 4 MeV were included in the average except that the $^{2}H(^{16}O,n)^{17}F$ reaction was included only once. A value $\bar{K} = 44.224$ keV·u/MHz^2 was obtained. The internal error, e_{int}, and external error, e_{ext}, are given by

$$e_{int} = (\sum W_i)^{-\frac{1}{2}};$$
$$e_{ext} = [(N-1)^{-1} \{\sum W_i (K_i - \bar{K})^2 / \sum W_i\}]^{\frac{1}{2}},$$

with N equal to the number of points. For these data, e_{int} and e_{ext} have values of 0.006 and 0.008 keV·u/MHz^2, respectively.

If the very low $^{27}Al(p,n)^{27}Si$ calibration point is excluded from the average, because it lies more than two standard deviations from the mean, the mean calibration factor becomes $\bar{K} = 44.230$ keV·u/MHz^2 with $e_{int} = 0.007$ and $e_{ext} = 0.006$ keV·u/MHz^2. Results of a χ^2 test applied to to this value, indicate that the experimental points are within the 50% confidence limit of this value of $\bar{K}$.

We have adopted the value $\bar{K} = 44.230 \pm 0.007$ keV·u/MHz^2. With this value of $\bar{K}$ a new, self-consistent set of threshold intercept energies can be calculated from the frequencies listed in table 1. This is a valid procedure if the reactions and their errors constitute a statistically valid sample and if all the reactions included are indeed a measure of the same magnet calibration constant. The results of these calculations are shown in table 2. The uncertainties listed were obtained by quadratically combining the uncertainties due to the threshold frequencies of table 1 with the standard deviation in $\bar{K}$. The recommendations of Marion[1]) are also shown.

TABLE 2
Self-consistent threshold energies.

Reaction	Threshold energy (this work) (keV)	Threshold energy (keV)[1])
$^{19}F(p,n)^{19}Ne$	4233 7 ± 0 7	4234.3 ± 0 8
$^{27}Al(p,n)^{27}Si$	5802.1 ± 1.0	5796.9 ± 3 8
$^{60}Ni(p,n)^{60}Cu$	7027.8 ± 1.6	7023.84 ± 3.9
$^{54}Fe(p,n)^{54}Co$	9204 1 ± 1.8	9202 7 ± 4 8
$^{58}Ni(p,n)^{60}Cu$	9511 0 ± 1 7	9515 2 ± 2 9

With the calibration and linearity of the analysis system established, a series of additional neutron threshold calibration points were determined. Since these results have appeared before[14]), they are merely summarized in table 3. Fig. 7 is typical of the data obtained in these measurements using the delayed positron detection methods[8]) as described above and shows the results of measurements on the $^{24}Mg(p,n)^{24}Al(\beta^+\nu)^{24}Mn$ reaction.

The $^{65}Cu(p,n)^{65}Zn$ reaction threshold has been used on occasion in the past as a calibration reaction, although no absolute measurement of the threshold energy has been made. The determinations which exist result either from threshold measurements relative to the $^{7}Li(p,n)^{7}Be$ and $^{13}C(p,n)^{13}N$ thresholds or from calculations using the ^{65}Zn β^+-end-point energy or

TABLE 3
Additional calibration reactions.

Reaction	Target	Threshold frequency (MHz)	Energy (keV)
$^{65}Cu(p,n)^{65}Zn$	evaporated foil	7.0275' ± 0 0005	2168.0 ± 0.8
$^{32}S(p,n)^{32}Cl$	evaporated S on gold	17.857 ± 0 010	13899 ± 14
$(^{32}S(p,n)^{32*}Cl)$		(17 914 ± 0.010)	(13987 ± 14)
$^{24}Mg(p,n)^{24}Al$	99% ^{24}Mg foil	18.734 ± 0 001	15286.3 ± 2.9
$^{40}Ca(p,n)^{40}Sc$	99 8U ^{40}Ca foil	18 860 ± 0 001	15491 1 ± 2.9
$^{28}Si(p,n)^{28}P$	quartz	18 969 ± 0 002	15668 9 ± 4 2
$^{12}C(p,n)^{12}N$	graphite	21 269 ± 0.002	19657.9 ± 4 8

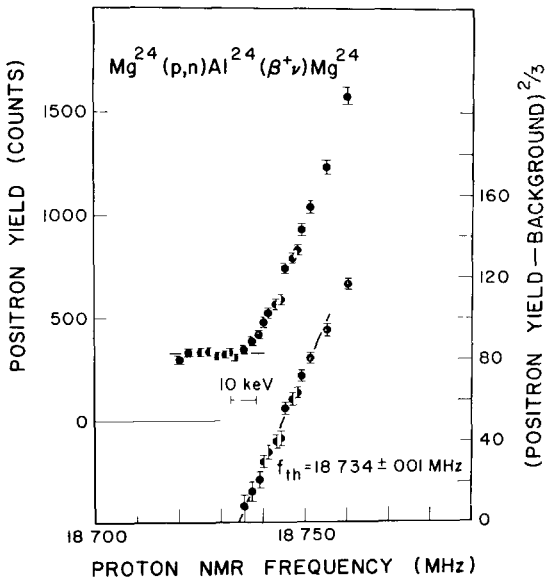

Fig 7 The $^{24}Mg(p,n)^{24}Al(\beta^+\nu)^{24}Mg$ delayed positron yield in the region of threshold. The indicated threshold frequency is shown as is the energy dispersion in this frequency range

measured neutron energies above threshold. Until 1956 these two types of results disagreed by about 5 keV, with the threshold measurements higher in energy, and it was conjectured that the disparity arose from resonant compound nucleus effects in ^{66}Zn which altered the neutron yield at threshold. However, in 1956 a threshold measurement was performed by Marion and Kavanagh[15]) with results which agreed with the threshold calculated from the β^+ end-point energy. Our calibration factor is not constant at these energies However, using a factor of 44.270 ± 0.015 keV·u/MHz^2, obtained by interpolation from the $^7Li(p,n)^7Be$ and $^{13}C(p,n)^{13}N$ thresholds, a threshold energy of 2168.0 ± 0.8 keV is obtained for the $^{65}Cu(p,n)^{65}Zn$ reaction. This is in agreement with other recent reports of 2168 ± 1.8 keV by Okano and Nishimura[11]) and of $2169\,0 \pm 1.7$ keV by Johnson et al.[16]) but is in disagreement with the value of 2165.3 ± 1.5 keV reported by Marion and Kavanagh.

The $^{32}S(p,n)^{32}Cl$ reaction proved to be the most difficult to study of those considered herein. A CdS target was first employed, but the β^+ yield above threshold was small, probably because of the high stopping cross section per sulfur atom in the target compound. Thereafter an elemental sulfur target was employed. Target deterioration under bombardment proved severe and it was difficult to obtain reproducible yields. The best curve obtained is shown in fig. 8. The threshold previously reported[14]) with the CdS target, corresponds to the second rise in fig. 6 and apparently is due to compound nucleus resonance structure or to a threshold due to an excited state of ^{32}Cl. If the latter is the case, the state has an excitation energy of approximately 85 keV ($E_{th} = 13.987 \pm 0.014$ keV). An excited state in ^{32}Cl at about 70 keV is expected from the level structure of the conjugate nucleus, ^{32}P. Previous evidence[17]) indicates that the ^{32}P ground and first excited states have spin and parity 1^+ and 2^+, respectively, while ^{32}Cl has ground state spin 2^+. Thus, these two lowest states in ^{32}Cl are inverted with respect to those in ^{32}P. This may well explain the enhanced yield at the first excited state, if the rise does indeed correspond to the first excited state of ^{32}Cl. An independent determination of the low level structure of ^{32}Cl would be of immediate interest.

Because of possible confusion resulting from excited states in the final nuclei, the $^{24}Mg(p,n)^{24}Al$, $^{28}Si(p,n)^{28}P$, and $^{40}Ca(p,n)^{40}Sc$ reactions were further investigated to energies several hundred keV above threshold. ^{24}Al is known[17]) to have an excited state at 437 keV, ^{28}P at 120 keV, and ^{40}Sc should have an excited state at about 30 keV, in analogy with that in ^{40}K. None of these states are inverted with respect to

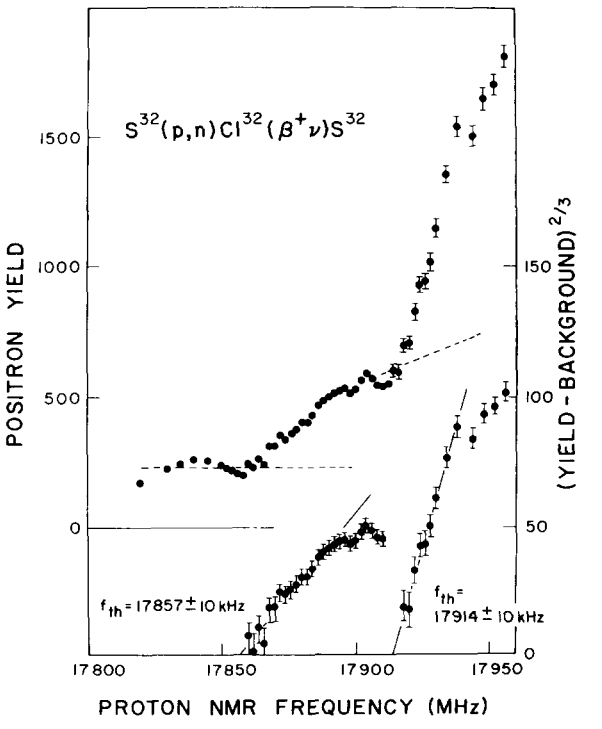

Fig 8 The $^{32}S(p,n)^{32}Cl(\beta^+\nu)^{32}S$ reaction near the neutron threshold Two thresholds are shown Backgrounds used to obtain the net yields are indicated by the dashed lines on the plot of the total yield.

the corresponding states in the conjugate nuclei. Although gentle undulations were observed in the corresponding yield curves, no additional thresholds were observed.

4. Conclusions

We believe that this constitutes a first attempt at combining energy standards from a variety of reactions into a self-consistent set of standards. If the process is a valid one, the resulting errors in the available standards are decreased significantly through the use of a larger statistical sample. Until further refinements of the absolute energy standards are available, it is hoped that the use of this self-consistent set will provide for the consistent calibration of additional accelerators.

Subsequent work with the established calibration has been encouraging. The $^{12}C(p,p)^{12}C$ reaction has been extensively studied in this laboratory by LeVine and Parker[18]) to investigate properties of the isobaric analogue states of ^{13}N. Detailed studies of the first $T = \frac{3}{2}$ state of ^{13}N near 14 MeV indicate a beam energy resolution, $\Delta E/E$, of 1.6×10^{-4}, consistent with the resolution estimated from the threshold studies at much lower energies. Their measured proton energy, at resonance, of 14.231 ± 0.004 MeV is in excellent agreement with the independent value of 14.233 ± 0.008 MeV which follows from the work of Adelberger and Barnes[19]) on the $^{11}B(^3He,n)^{13}N$ reaction. Additional confirmation of these calibration procedures is provided by the excellent agreement between the $^{12}C(p,n)^{12}N$ threshold energy measured here, 19.658 ± 0.005 MeV, and the value of 19.661 ± 0.005 MeV derived independently from $^{10}B(^3He,n)^{12}N$ Q-value measurements[20]).

The calibrations have been found to be constant and reproducible over the period of two years since the initial installation and calibration of the Yale facility.

It is a particular pleasure to thank Professor H. H. Barschall for his advice and contributions to this study during the six months which he spent at Yale in 1966.

We wish to thank Mr. K. Sato and his operating group and Mr. C. E. L. Gingell and his instrumentation group for their extensive and indispensable assistance during the course of these measurements. Messrs. R. Fernald, J. Scotney and W. Sheer of the High Voltage Engineering Corporation participated in the early phases of this work and their help was invaluable in bringing a new accelerator type into operation. Messrs. R. Hirko, G. Holland, M. LeVine, B. Skwiersky, H. Shay and W. Thompson assisted in the collection of data.

References

1) J. B Marion, Rev. Mod. Phys **38** (1966) 660
2) D W. Palmer, W. G. Mourad, J. M Donhowe, K. E. Nielsen and R J Nickles, Nuclear Physics **75** (1966) 515
3) R. O. Bondelid and E E D Whiting, Phys Rev **134** (1964) B591.
4) E. H. Beckner, R L Bramblett, G. C Phillips and T A. Eastwood, Phys Rev. **123** (1961) 2100.
5) A Rytz, H. Winkler, F. Zamboni and W Zych, Helv Phys. Acta **34** (1961) 819
6) B E. Bonner, G Rickards, D L Bernard and G. C Phillips, Nuclear Physics **86** (1966) 187
7) G Murray, J M. Freeman, J G Jenkin and W E Burcham, *Recent Progress in Nuclear Physics with Tandems*, Symposium Proc (unpublished, ed W Hering; Heidelberg, W Germany, 1966)
8) J. M Freeman, J H Montague, G. Murray, R E White and W E. Burcham, Nuclear Physics **65** (1965) 113.
9) R O. Bondelid, J W Butler and C. A Kennedy, Phys Rev **120** (1960) 889
10) J H E Mattauch, W Thiele and A H Wapstra, Nuclear Physics **67** (1965) 1
11) K Okano and K. Nishimura, J. Phys Soc Japan **18** (1963) 1563
12) J. D. Kington, J K. Bair, H. O Cohn and H B Willard, Phys Rev **99** (1955) 1393.
13) D. A. Bromley, E Almqvist, H E Gove, A J Ferguson, J A Kuehner and A E. Litherland, Can J Phys. **37** (1959) 1514
14) D A Bromley, J C Overley and P D Parker, Phys Rev. Letters **17** (1966) 705.
15) J B Marion and R W. Kavanagh, Phys Rev **104** (1956) 107.
16) C H Johson, C C Trail and A. Galonsky, Phys Rev **136** (1964) B1719
17) P M Endt and C. Van der Leun, Nuclear Physics **A105** (1967) 1
18) M. J LeVine and P D Parker, to be published
19) E. G Adelberger and C A. Barnes, Bull Am Phys Soc **10** (1965) 1195
20) F. Ajzenberg-Selove and T. Lauritsen, Nuclear Physics **A114** (1968) 1